JGR Oceans

RESEARCH ARTICLE
10.1029/2020JC016588

This article is a companion to Shen et al. (2021), https://doi.org/10.1029/2020JC016587.

Key Points:

- We undertake novel experiments to quantify the evolution of an underwater gas eruption and its free surface response
- Three types of fountain regimes observed in our experiments are consistent with field observations of underwater volcanic eruptions
- Finger regimes occur at shallow depths or in the eruptions with strong source energy, while dome regimes occur under the opposite conditions

Supporting Information:

Supporting Information may be found in the online version of this article.

Correspondence to:

Y. Shen,
yshe948@aucklanduni.ac.nz

Citation:

Shen, Y., Whittaker, C. N., Lane, E. M., White, J. D. L., Power, W., & Nomikou, P. (2021). Laboratory experiments on tsunamigenic discrete subaqueous volcanic eruptions. Part 1: Free surface disturbances. *Journal of Geophysical Research: Oceans*, *126*, e2020JC016588. https://doi.org/10.1029/2020JC016588

Received 9 JUL 2020
Accepted 24 MAR 2021

Laboratory Experiments on Tsunamigenic Discrete Subaqueous Volcanic Eruptions. Part 1: Free Surface Disturbances

Yaxiong Shen[1], Colin N. Whittaker[1], Emily M. Lane[2], James D.L. White[3], William Power[4], and Paraskevi Nomikou[5]

[1]Department of Civil and Environmental Engineering, University of Auckland, Auckland, New Zealand, [2]National Institute of Water and Atmospheric Research (NIWA), Christchurch, New Zealand, [3]Department of Geology, University of Otago, Dunedin, New Zealand, [4]GNS Science, Lower Hutt, New Zealand, [5]Department of Geology and Geoenvironment, National and Kapodistrian University of Athens, Athens, Greece

Abstract

A submarine volcanic eruption has the potential to generate a dangerous local tsunami. To better understand the free surface disturbance generated by an underwater volcanic eruption, which will form the initial condition for any subsequent wave generation, we conducted a series of laboratory experiments. In these experiments, compressed air was injected into a tank filled with water to simulate an underwater eruption. The experiments were repeated over a range of different pressures and water depths. Each eruption can be divided into three phases: A momentum-driven jet, a buoyancy-driven plume, and a fountain-generation regime. Our experiments exhibit two fountain regimes (a dome regime and a finger regime), with a transition between them. These fountain regimes have been observed in several real submarine volcanic eruptions. This paper proposes a Froude number criterion to combine the water depths and source conditions together with the aspect ratios of fountains to quantify different fountain regimes. This quantitative relationship holds for two real subaqueous volcanic eruption cases (Myojin-Sho eruption in 1952 and 1996 eruption in Karymskoye Lake). The fountain of the Myojin-Sho shallow submarine eruption on September 23,1952 appears to have been in the dome regime, which means it was a relatively weak eruption. Unlike other eruptions from this volcano, which did generate tsunamis, no tsunami waves were detected on September 23 . This study contributes to an enhanced understanding of the usually unseen mechanism of free surface disturbances by volcanic gas injection during submarine eruptions.

Plain Language Summary

Underwater volcanic eruptions inject hot magma into cold ambient water. The interaction between magma and water creates steam explosions which can displace a large amount of water. An eruption occurring in shallow enough water and with sufficiently strong energy will be able to disturb the water surface and even initiate a tsunami. As these eruptions are hidden beneath water, their direct observation near their vents is difficult and dangerous, while the water surface disturbances are much easier and safer to measure. In order to understand the relationship between different kinds of eruptions and their disturbance of the water surface, we model underwater volcanic eruptions in the laboratory by injecting compressed air into water. We observe three main shapes of fountains on the water surface in our experiments: a) finger-like; b) dome-like; c) shapes intermediate between them. A finger-shaped fountain accompanied by a large number of splashes normally occurs at shallow-water depths and/or in an eruption with intense source strength, while a dome-shaped fountain occurs under the opposite conditions. We find a good consistency between our experimental results and field observations, which means that we are able to estimate the unseen source conditions from the observed free surface disturbances.

1. Introduction

Over 75% of annual magmatic outputs come from submarine volcanic eruptions, but these eruptions account for only 8% of all recorded eruptions (Cashman & Fiske, 1991; Day, 2015; Mastin & Witter, 2000). Most submarine eruptions occurring 500 m or more below the surface do not disturb the water surface (Latter, 1981). However, a small number of eruptions are in shallow enough water and are sufficiently

strong that they are not only able to disturb the water surface but to generate a tsunami. For example, the submarine eruption of Kolumbo volcano in 1650 triggered a tsunami that generated localized runup as high as 15 m and killed about 20 people (Day, 2015; Fouqué, 1879). The eruption of Myojin-Sho destroyed *Kaiyo Maru 5*, a Japanese research vessel that was investigating the eruption near the source, causing 31 deaths on September 24, 1952 (Dietz & Sheehy, 1954). This demonstrates that submarine volcanic eruptions can generate dangerous free-surface disturbances under certain conditions.

There have been a few relatively well-observed submarine volcanic eruptions, which can provide us with some information about general mechanisms of a submarine volcanic eruption. Stehn (1929) first recorded several submarine explosions of Anak Krakatau breaching the surface in 1927. The submarine Kavachi volcano was first observed in 1939 and it has frequently erupted in recent decades. There are some scattered photos, videos and ASTER satellite images recording some of these eruptions (Global Volcanism Program, 2014). The Myojin-Sho volcano erupted several times in September,1952 and two eruptions on September 23 were recorded in a series of photos (Miyoshi, 1955; Morimoto, 1960). The wave and acoustic pressure data associated with this series of eruptions were detected by a wave gauge in Hachijo Island and a U.S. Navy Sofar station at California, respectively (Dietz & Sheehy, 1954; Nakano et al., 1954). V. Bahtiarov recorded video of one of the strongest sublacustrine volcanic explosion in Karymskoye lake in 1996 (Muraviev et al., 1997) and a field survey collected tsunami wave runup data around the coastline of the lake after the event (Belousov & Belousova, 2001). There are only two small subaqueous volcanic eruptions that have been observed at their vents (NW Rota-1, Mariana arc and West Mata, Tonga arc), which have provided valuable information to understand the specific mechanisms at the source (Resing et al., 2011; Walker et al., 2008). In reality, no complete data-set has been recorded of a submarine volcanic eruption from the source dynamics to the water-volcanic substance interactions to free surface disturbances. Laboratory experiments provide a comprehensive and high-quality data-set, which can enhance the understanding of tsunamigenic submarine volcanic eruptions.

Volcanic eruptions may be discrete or sustained. Most previous experimental and theoretical studies have ignored unsteady source conditions and assumed constant discharge rates (i.e., sustained eruptions) for simplicity (Sangras et al., 2002; Witze, 1983). In reality, discrete eruptions with strong and sudden variations in source properties happen frequently (Chojnicki et al., 2015). Therefore, this study investigates discrete underwater eruptions and free surface responses.

Subaqueous explosive eruptions are complicated phenomena that are challenging to replicate in physical experiments. Previously they have been conceptualized as phenomena within a spectrum ranging from explosions (Bernard & Shen, 1996; Stepanov & Navagin, 1966) to water jets (Chojnicki et al., 2015; Maurel et al., 1997), with gas jets as an intermediate case (Bie et al., 2016; Verolino et al., 2018).

In submerged explosion experiments, there are three important parameters determining the characteristics of free surface disturbances: yield (expressed in pounds of TNT equivalent for high explosives, and conceptually the same as explosion energy), explosion depths, and water depths (Kedrinskiy, 2006). Stepanov and Navagin (1966) performed experiments to study the formation of fountains caused by an underwater explosion. In their experiments, a trap height 2.4 m above the water surface collected splashes during the explosions. They found that there was a critical explosion depth at which an explosion could generate the maximum displaced water. However, the kinematic and dynamic mechanisms between explosions and eruptions are different. Energy and materials propagate along a dominant direction in eruptions, while they spread radially in all directions from a blasting source. In the NW Rota-1 and West Mata eruptions, the eruptive activities were driven primarily by the expansion of magmatic gases and the explosive activities were rare and weak (Chadwick Jr et al., 2008; Resing et al., 2011). True explosions may happen during submarine volcanic eruptions, but even where they do they will take place in or on the volcano rather than in the water column. For this reason, we consider submerged jets to be more representative of such underwater volcanic eruptions than underwater explosions.

A water jet experiment is the most common type used to study a subaqueous eruption because of its high repeatability. The experiments of Maurel et al. (1997) were among the few that have studied the water surface motion generated by a vertical confined jet. For increased velocity or decreased depth, the surface disturbance changed from a stationary bump, to a self-sustained oscillation regime, to an oscillation with a

frequency spectrum. Chojnicki et al. (2015) conducted a systematic investigation on the impulse jets generated by unsteady sources, to simulate subaerial volcanic plumes. They found that the time-dependent vertical location of the jet front could be expressed in a logarithmic curve based on their experimental data and theoretical analysis. In the NW Rota-1 eruption, both momentum-driven phases and buoyancy-driven phases were observed during plume rise, and the surrounding water strongly inhibited the eruption plumes (Deardorff et al., 2011). Although buoyancy-driven behaviors can be simulated by liquid jets with a sufficient density difference from the ambient fluid, the compressibility of a gas plume still cannot be reproduced by liquid jet experiments.

Gas jet experiments lie between the other two experimental types in their ability to capture some essential characteristics of both plume motion and expansions, such as compressibility, momentum-driven behaviors, and buoyancy-driven behaviors. In this approach, high-pressure gas is suddenly released, resulting in volume expansion and eruption. Bie et al. (2016) studied submerged exhaust noise produced by underwater gas injections. They determined that the Weber number could be used to define a threshold condition at which jet flow changed from a jetting regime to a bubbling regime, and demonstrated this both theoretically and experimentally. Verolino et al. (2018) modeled subaqueous volcanic eruptions at laboratory scale by injecting compressed argon through volcanic ash or other particles to produce gas-particle eruption mixtures. Observations and measurements of the rise behaviors of dry particles jetting into water agreed well with observations of submarine volcanic plumes at NW Rota-1, Mariana arc (Walker et al., 2008).

Most of the studies summarized above focused on the properties of the underwater eruptions, but ignored the fountains generated on the free surface. In fact, the perturbations to the water surface can directly cause damage to near-source regions and, subsequently, waves can spread the damage to a far greater area (e.g., Myojin-Sho 1952). Therefore, it is critical to understand both the characteristics of underwater eruptions and how they relate to free surface responses.

This paper uses physical experiments to describe the phases of underwater volcanic eruptions and investigates their free surface responses. For a fixed orifice diameter, we investigate how pressure and water depth affect the source volume, source velocity, jet-plume-fountain front path and boundaries of the jet-plume and the fountain. There are three kinds of fountain regimes (dome, transitional, finger) that vary with the Froude number (Fr) in our experiments. These three fountain regimes are consistent with the surface disturbances of some observed submarine volcanic eruptions. The relationship between the fountain regimes and Fr in our experiments agrees well with the available field data from the Myojin-Sho eruptions in 1952 and sublacustrine eruptions in Karymskoye lake in 1996.

2. Experimental Facility and Scaling

2.1. Setup

We simulated tsunamis generated by subaqueous eruptions in a water tank which is 1.43 m long, 0.88 m wide and 0.88 m high (Figure 1). A circular orifice with a diameter, d_0, of 0.013 m is located at the bottom center of the tank. Air is supplied from the cylinder to generate a maximum initial pressure of up to 1,000 kPa (gauge pressure). A pressure transducer records pressure data, $p(t)$, just below the orifice, at a frequency of 400 Hz. The minimum switching time of the solenoid valve is 0.1 s. Images of eruptions are recorded by a Phantom Digital high-speed video camera with 1,000 fps frequency and 1,280 × 720 pixel resolution. A Nikon AF NIKKOR 50 mm f/1.4D Lens employed in our experiments can deliver distortion-free images with only ambient lighting. In each run, we start with valve 2 open and valve 1 closed. Then, we adjust the regulator to fill the tube with the compressed air at a specific pressure, p_0. Finally, we close valve 2 and open valve 1 for a specified eruption duration, $\triangle t$, to release the gas into the water. The volume of the tube, V_0, is 0.00042 m^3. If an eruption process is assumed to be an isothermal process and follows the ideal gas law, we calculate the total volume (at normal temperature and atmospheric pressure) of the released gas during the eruption, V_g,

$$V_g = \frac{p_0 V_0 - p_e V_0}{p_a} \tag{1}$$

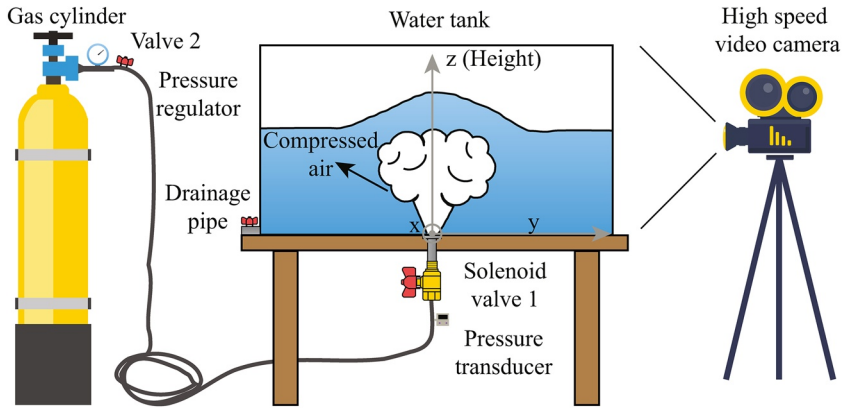

Figure 1. A schematic of the experimental setup used to generate high-pressure gas eruptions including a coordinate system. The direction of the *x*-axis is perpendicular to the plane of the paper.

and the mean velocity of the eruption, $\overline{v}$,

$$\overline{v} = \frac{4(p_0V_0 - p_eV_0)}{\pi d_0^2 \overline{p} \triangle t} \tag{2}$$

where p_e is the pressure in the tube after the eruption, p_a is the atmospheric pressure, $\overline{p}$ is the mean pressure of the tube during the eruption; $\triangle t$ is the eruption duration.

2.2. Scaling

The source conditions and water depths of real submarine volcanoes vary greatly. The key variables in our experiments are initial source pressures p_0 and water depths d. In terms of field measurements, no data on source pressures during submarine eruptions are available. Some acoustic records in the far-field can provide some information about the eruptive strengths, starting times, and durations, but these data cannot be translated to the initial source pressures directly. Explosive volcanic eruptions have been inferred to involve volcanic gas pressures estimated between 50 and100 MPa (Mader et al., 1994), whereas Wohletz and McQueen (1984) report pressures exceeding 35 MPa for volcanic explosions driven by thermohydraulic magma-water interactions, called fuel-coolant interactions (Wohletz, 1986). Latter (1981) suggests that tsunamis normally would be generated when eruptions occur at water depths equal to or shallower than 500 m, at which the hydrostatic pressure is a few megapascals. Thus, if we assume the source initial pressure is similar to the volcanic gas pressures or those from explosive magma-water interactions, the ratio of the source initial pressure to ambient hydrostatic pressure is larger than 7:1. In our experiments, the ratio of pipe pressure to ambient hydrostatic pressure in the tank (between 2:1 and 4:1) is less than in the field, but these eruptions disturb the free surface. Water depths in our experiments vary from 0.3–0.6 m, allowing the study of both jet-plume motion behavior and fountain generation at the water surface. Hydrostatic pressure increases at a rate of about 980 kPa per 100 m water depth. In observed submarine volcanic eruptions, the hydrostatic pressure can be tens of times higher than in our experiments. The increased hydrostatic pressure with increasing water depth would inhibit gas expansion and suppress the energy of the eruption (Walker et al., 2008), which is not considered in our experiments. The eruption time (defined as the valve opening time) during our experiments is 0.1 s to simulate short-lived, discrete, "explosive" bursts. A short-lived and discrete eruption, in our experiments, formed when the time that the valve remains open is much shorter than the rise time of jet-plume-fountain. In our experiments, the ratio of the opening time of the valve and the rising time of jet-plume-fountain is between 0.10 and 0.29, which is sufficiently smaller than 1 to be considered "short." In our experiments, we use cool non-condensable gases, which cannot reproduce the heat exchange between real volcanic gases and ambient water. This difference in driving gas influences the mechanism of interaction between eruption materials, the eruption jet, and ambient tank water, with implications for the subsequent fountain generation. Specifically, condensation of water vapor would decrease gas volume after injection (Verolino et al., 2018).

Table 1
Summary of Initial Conditions, Source Volumes (Equation 1), Velocities (Equation 2), Froude Number (Equation 3), and Fountain Aspect Ratio (Equation 4)

Experiment name	Initial pressure (kPa)	Water depth (m)	Eruption duration (s)	Mean calculated gas volume and its standard deviation (L)	Mean calculated source velocity and its standard deviation (m/s)	Mean calculated Froude number	Mean calculated fountain aspect ratio
Test 1	100	0.5	0.1	0.29 (0.015)	13.0 (1.2)	5.9	0.28
Test 2	200	0.5	0.1	0.67 (0.022)	17.4 (1.2)	7.9	1.10
Test 3	300	0.5	0.1	1.09 (0.018)	22.4 (1.0)	10.1	1.18
Test 4	100	0.3	0.1	0.32 (0.029)	14.3 (0.9)	8.3	1.00
Test 5	100	0.4	0.1	0.28 (0.023)	13.4 (1.0)	6.8	0.66
Test 6	100	0.6	0.1	0.29 (0.023)	13.3 (1.2)	5.5	0.24
Test 7	300	0.3	0.1	1.07 (0.023)	22.8 (1.3)	13.3	2.30
Test 8	300	0.4	0.1	1.09 (0.021)	22.1 (0.7)	11.2	1.88
Test 9	300	0.6	0.1	1.07 (0.017)	22.1 (0.8)	9.1	1.13

The reproduction of the geometric dimensions of volcanoes, such as vent length and diameter, is also difficult in the laboratory (Mader et al., 1994), and those dimensions are also very poorly defined for submarine volcanoes. Previous laboratory experiments indicate that the vent diameter needs to be much larger than the diameter of the smallest bubble or particle, so that it does not affect the interactions between phases (Mader et al., 1994; Verolino et al., 2018). Compared with previous laboratory experiments (Clarke et al., 2009; Mader et al., 1994; Maurel et al., 1997; Verolino et al., 2018), the geometric size of equipment in our experiment is much larger, allowing acceptable generation of plumes. In general, although our setup is not rigorously downscaled from real volcanoes, it provides valuable insights to analyze plume motion, fountain generation and the relationships between them.

3. Methods

3.1. Experimental Groups

We performed nine experiments over a range of water depths and source initial pressures (Table 1). To average out the randomness of jet-plume motion and splashing, each experiment was repeated at least nine times. In this paper, we show the average and the standard deviations of the multiple individual runs that comprise each experiment.

3.2. Jet-Plume and Fountain Boundary-Detecting Algorithm

The jet-plume and fountain boundaries between the air and water were recorded by a Phantom high-speed camera and extracted in MATLAB®. The recording time is 1 s for all videos, as the collapse of the fountain is completed and the subsequent waves start to radiate away from the source after 1 s. The uncertainty for measurements of the boundary is less than 1.6 mm. As the images exhibit very little distortion (mean projection error is 0.12 pixels based on the Camera Calibration Toolbox in MATLAB®), correcting lens distortion is not considered in image analysis. The maximum error caused by the depth of the field is less than 2%, so the depth correction is also not included in image analysis. We developed two different algorithms to detect jet-plume boundaries and fountain boundaries, respectively. The jet-plume boundary-detecting algorithm is based on Bombrun et al. (2018). The steps of the jet-plume boundary-detecting algorithm and fountain boundary-detecting algorithm are given in supporting information Text S1 and Text S2, respectively. If there are other moving objects in the video, such as shadows or reflections, the algorithm would need to be further improved to exclude disturbances in detecting jet-plume or fountain boundaries.

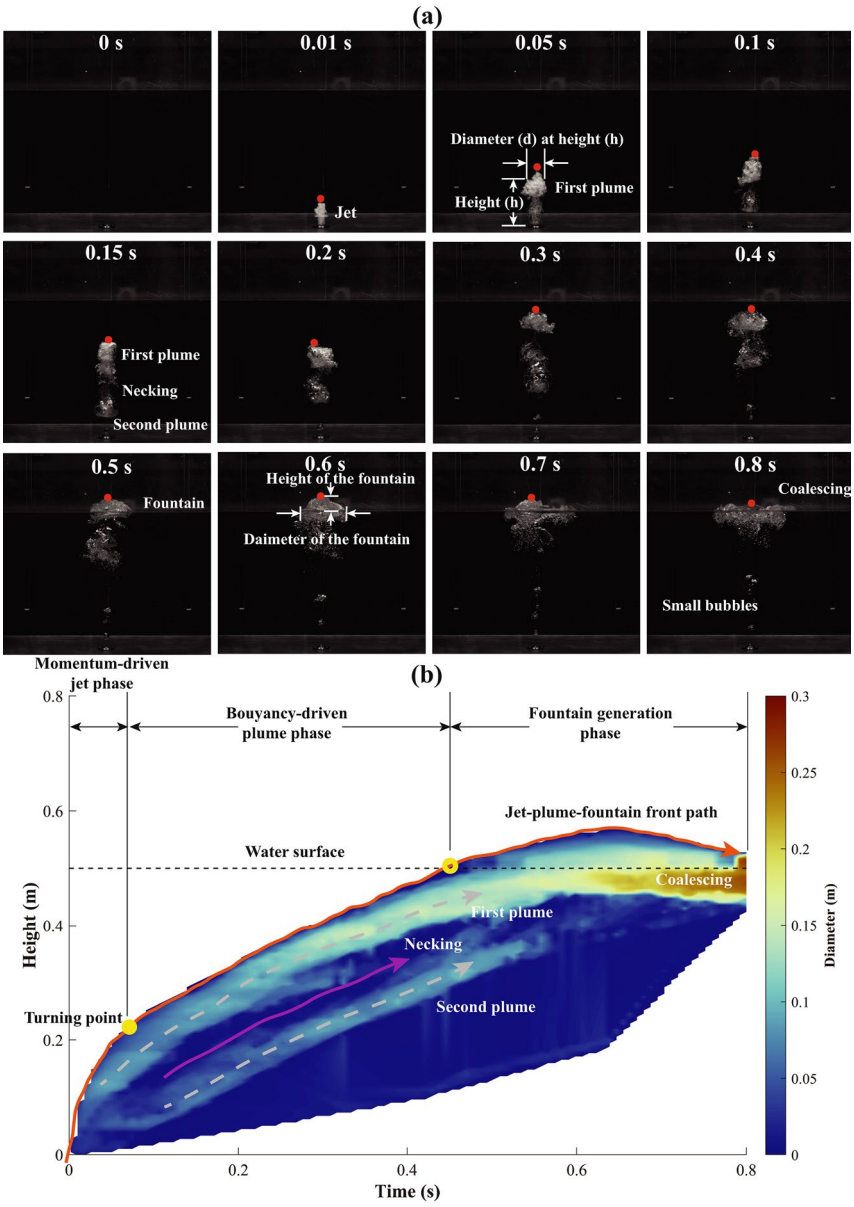

Figure 2. Overview of the process of an eruption; (a) The time sequence of an eruption in Test 1 (water depth: 0.5 m, pressure: 100 kPa, and eruption duration: 0.1 s); (b) Quantification of the eruption process recorded by the video.

4. Results and Discussion

4.1. Eruption Process

One run of Test 1 is used as an example to show the whole process of an eruption in our experiments (Figure 2a). At first (0.01 s), the shape of the jet is narrow and the jet expands rapidly in the vertical direction. Then, the vertical expansion slows and the jet broadens as it transforms into a plume (0.05 and 0.1 s). After that, the first plume separates from the source and the second plume is generated with a necking region between them (from 0.15 to 0.4 s). The first plume and second plume eventually coalesce and generate a fountain on the water surface (from 0.5 to 0.8 s). After 0.8 s, only some small bubbles follow; however, these have no effect on water surface motion. The complete video of this eruption is given in supporting information, Movie S1.

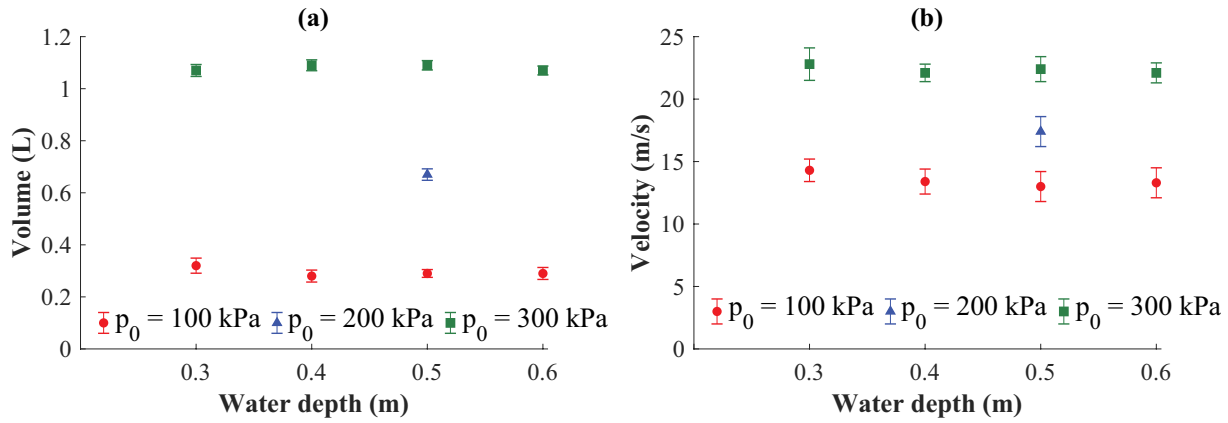

Figure 3. Source volumes (a) and average velocities (b) at different source initial pressures and water depths. Scatters show means and whiskers show ± one standard deviation.

We quantify the evolution of the eruption recorded by the high-speed camera (Figure 2b). Each colored point represents the jet-plume diameter at a given time and height (defined in Figure. 2a 0.05 s). Two plumes (gray dashed arrows) and one necking event (purple arrow) occur during this eruption. The first plume is the main one, with the volume of the second plume being smaller. The orange arrow represents the jet-plume-fountain front path of the eruption. The jet-plume-fountain front path is obtained by the top points (red dots in Figure 2a) of the jet-plume-fountain in each time step. There are three main phases to the eruption, with the transition between them indicated by a yellow dot and a yellow circle. The first transition occurs at the clear turning point (yellow dot) on the jet-plume-fountain front path at approximately 0.04 s. The gradient of the front decreases sharply at this point, as the main driving force transitions from momentum to buoyancy. Hence, the first two phases of eruptions are named the momentum-driven jet and the buoyancy-driven plume, respectively. Necking also happens at this turning point, because the first plume separates from the source at this time. The second transition occurs when the jet-plume-fountain front path intersects the water surface (yellow circle). After that, fountains are generated, so the third phase is called the fountain-generation phase. The general features of this quantitative record are consistent over the parameter space tested in these experiments.

Previous research (Verolino et al., 2018) only qualitatively depicted eruption processes and largely ignored the processes after the plumes reached the water surface because of their narrow tank. Necking was also observed in other experiments by using gas jetting into water (Verolino et al., 2018), but it did not occur in the experiments in which the jetting material is the same as the ambient medium, as these experiments did not contain a buoyant plume (Alatorre-Ibargüengoitia et al., 2011; Chojnicki et al., 2015). Necking may be due to the unsteadiness of the interface between gas and liquid, the density difference between them, and the pressure variation in the orifice and near field region of the jet flow (Ozawa & Mori, 1986; Wraith & Chalkley, 1977).

4.2. Repeatability

An underwater gas eruption is a very turbulent phenomenon and there is significant randomness in the gas expansion and its interaction with the ambient water. We present the mean and the standard deviation of the released gas volumes and velocities at the source for different pressures and water depths in Figure 3. The volumes are calculated under the assumption of room temperature and atmospheric pressure (Equation 1). The average velocities (Equation 2) are subsequently calculated by dividing the gas volumes at the mean pressures during the eruption by the eruption duration and the area of the orifice. The water depths and pressures have very little impact on the standard deviation of gas volumes and velocities (Figure 3).

The standard deviation of the front heights slightly increases during the stage of jet-plume ascent, then increases more markedly during the ascent of the fountain and finally decreases during the descent of the fountain (Figure 4). There is a large amount of splashing after the air-water mixtures exit the water surface,

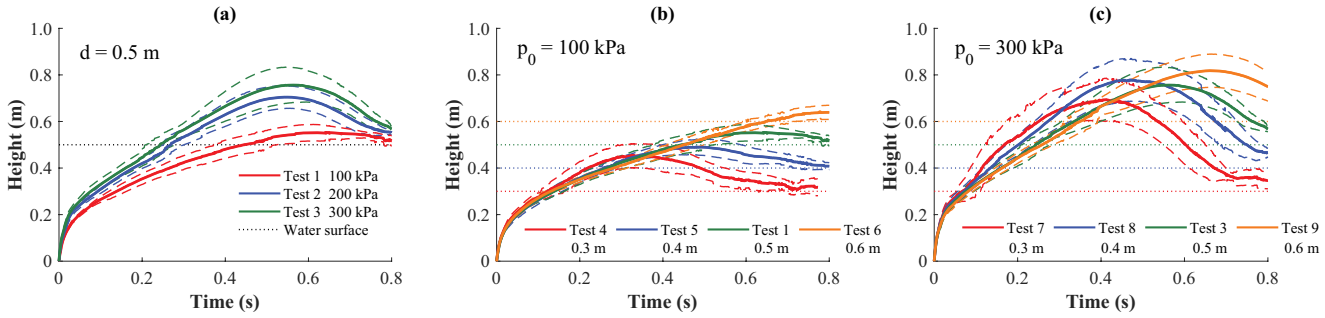

Figure 4. Time evolution of the jet-plume-fountain front heights varying with initial pressures (a) and water depths (b and c). The solid line represents the mean value of the front heights, the dashed line shows ± one standard deviation around the mean values. Horizontal dotted lines represent the water surface.

and the high randomness of the splash motion will further increase the variance in the results. The standard deviation of the front heights at high initial pressures is slightly larger than the deviation at low initial pressures (Figure 4a). Similar conclusions can also be drawn by comparing Figures 4b and 4c. Increasing the initial gas pressure increases the volume of the gas jetting into the water (Table 1), and thus results in greater standard deviation (Figure 4a). These figures also indicate that the front heights are more variable in shallow water depths. At a given source pressure, increasing the water depth reduces splashing at the water surface, thereby reducing the standard deviation (Figures 4b and 4c). Maurel et al. (1997) also observed that decreasing water depths or increasing jetting velocities led to a less stable oscillation of the bump on the water surface, in their experiments using a submerged water jet impinging on the water surface. The repeatability of the jet-plume-fountain boundaries is similar to the repeatability of jet-plume-fountain front heights.

4.3. The Effect of Gas Pressures and Water Depths on Source Volumes, Source Velocities, Jet-Plume-Fountain Front Paths, Jet-Plume Boundaries, and Fountain Boundaries

4.3.1. Source Volumes and Source Velocities

Initial gas pressures strongly affect the source velocities and volumes of gas, with both the source velocities and gas volumes increasing with higher initial gas pressures (Figure 3). There does not appear to be a significant relationship between water depths and either volumes or velocities, because the hydrostatic pressure in our experiments is very low, even at the maximum water depths (0.6 m). In reality, submarine volcanic eruptions take place at depths of up to a few kilometres, where the hydrostatic pressure is much larger. Because, however, it is actually the balance of pressure, not the absolute value, that is most important, the gas jet experiment is still an effective approach to simulate a natural submarine volcanic eruption (Verolino et al., 2018).

4.3.2. Jet-Plume-Fountain Front Paths

Tracking through time the evolution of the leading front of the jet-plume-fountain is a common method to describe the motion of jet-plume-fountains, widely used in previous experimental studies (Chojnicki et al., 2015; Verolino et al., 2018) and field data analysis (Deardorff et al., 2011). In our experiments, all the jet-plume-fountain front heights increase first and then decrease, corresponding to the air-water mixture erupting out of the water surface, generating spray and then falling (Figure 4). In the buoyancy phase, the front velocities of the tests with high initial pressures are slightly larger than those of the tests with low initial pressures (Figure 4a), which means the inertial force still has a slight impact on the motion of plume in this stage.

Chojnicki et al. (2015) combined theoretical and physical models to demonstrate a logarithmic time dependence for the advance of an unsteady neutrally buoyant jet (water injected into water). This theoretical model is not applicable for our experiments (gas injected into water), because our experiments include two separate phases, compressibility and buoyancy forces, which are much more complicated than the theoretical model.

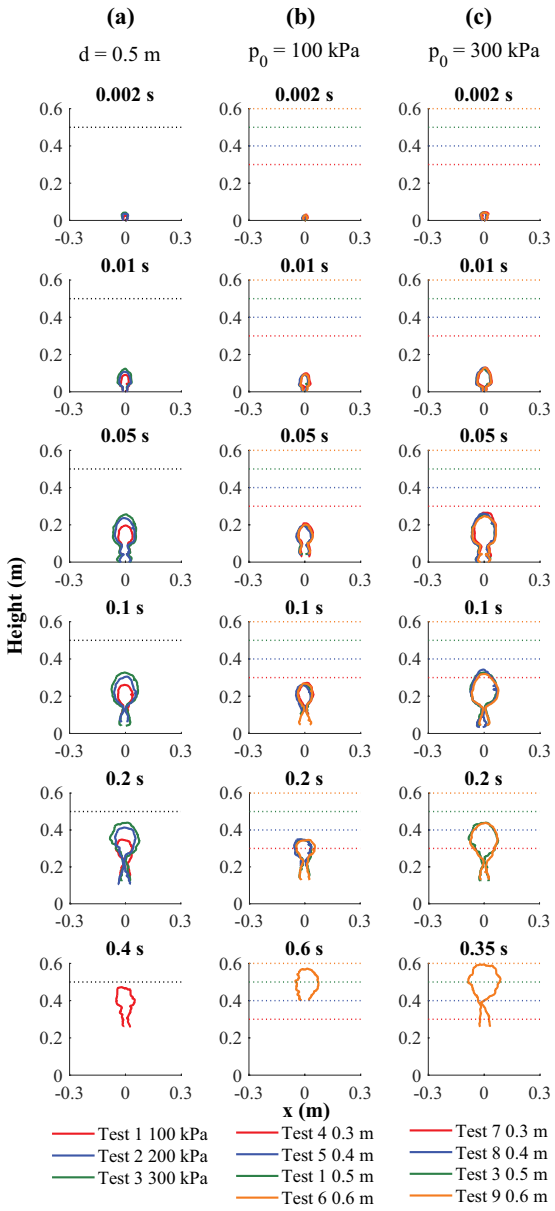

Figure 5. The mean jet-plume boundaries at different initial gas pressures (a) and water depths (b) and (c); solid lines, mean eruption boundaries, horizontal line, water surface. The color of the water surface in (b) and (c) corresponds to the color of each test in (b) and (c), respectively.

4.3.3. Jet-Plume Boundaries

The eruptions in the experiments with high initial pressures expand more rapidly in both horizontal and vertical direction than the lower-pressure eruptions (Figure 5a). For the experiments with different water depths and similar pressures, the evolution of the shapes and sizes of the jet-plume boundaries are almost identical below the water surface (Figures 5b and 5c). We can infer that if the water depth were infinite, there would be a complete evolution of the plume motion (from a momentum-driven jet to a buoyancy-driven plume). The water surface, however, terminates the evolution of the jet-plume, whereupon the fountain is formed. In all experiments, the size of the main plume near the water surface is larger in the deeper and higher-pressure cases (Figure 6). As expected, for the larger water depths or the lower pressures, the plumes need a longer time to reach the water surface, t_{surf}.

4.3.4. Fountain Boundaries

There are three main shapes of the fountain in our experiments (Figure 6): 1) vertical fingers, such as Tests 7 and 8; 2) domes or hemispheres, such as Tests 1, 5, and 6; 3) transitional shapes between vertical fingers and hemispheres, such as Tests 3, 4 and 9. Supporting information provides three videos corresponding to these three fountain regimes (a dome regime in Movie S1, a transitional regime in Movie S2, a finger regime in Movie S3). The dome regime occurs with the conditions of deep-water depths and/or low initial pressures, while the finger regime occurs in the opposite conditions (Figure 6).

In a dome regime, the shape of the fountain is wide at the bottom, and the height of the fountain is low (Figure 7). There is no splash during the ejection, and all the water is contained during the falling stage. The diameter of the bottom of the fountain continuously grows during the whole process, and waves propagate radially from the center. When a fountain erupts in the finger regime, there is a high and narrow fountain with a large number of irregular splashes (Figure 7). It takes a longer time to fall back to the water because of the height of the fountain. Some droplets fall far away from the center, which dissipates a large amount of energy. In finger regimes, waves are mainly generated by the fountain falling to the free surface. Some droplets falling far away from the center would also generate some small waves which may slightly impact the wavefield. The third regime (not shown in Figure 7) is an intermediate case and has the characteristics of both the dome and finger regimes.

Both water depths and initial pressures influence the regime in which a fountain occurs. A large eruption in deep water may produce a similar shape of the fountain at the surface as would a smaller eruption in shallow water, such as Test 4 and Test 9. Therefore, it is valuable to put forward a non-dimensional parameter to quantify the initial condition, including source intensity (whereby energy is imparted to the fountain on the free surface) and water depth (working as the resistance to dissipate energy during the jet-plume motion), and a parameter to quantify the regime. The Fr is a dimensionless number defined as the ratio of the inertial force to the gravitational force (Equation 3).

$$Fr = \frac{u_0}{\sqrt{g l_0}} \tag{3}$$

where u_0 is a characteristic flow velocity, g is gravitational acceleration, and l_0 is a characteristic length. There are various forms of Fr applied to different situations by selecting different characteristic flow velocities and

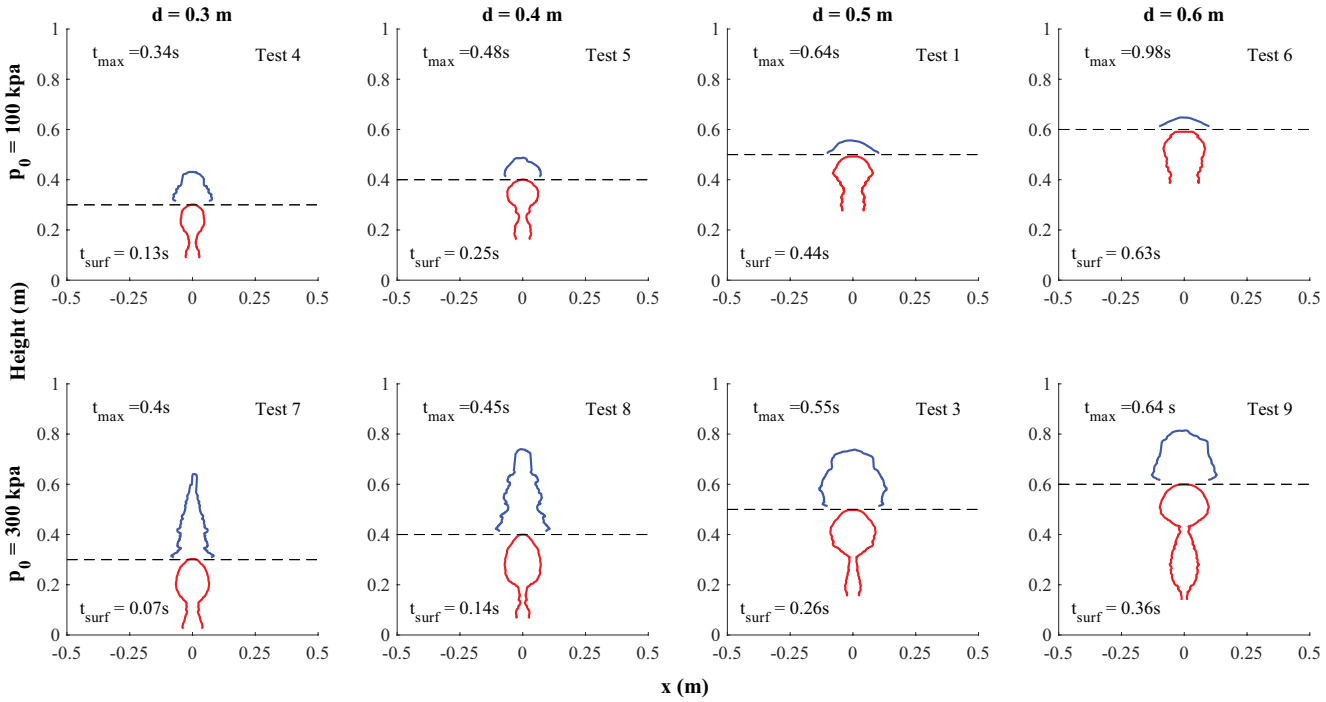

Figure 6. The jet-plume boundaries (red line) at the time when the jet-plume made the first contact with the water surface (horizontal dashed line) and the highest fountain boundaries (blue line) at the different initial gas pressures and water depths.

characteristic lengths. For example, in open-channel flows, if water depth and the average fluid velocity are selected as the characteristic length and velocity, the Fr can classify the flows as being supercritical, critical or subcritical (Munson et al., 2013).

In our case, we select the mean source velocity (Equation 2) and water depth as the characteristic flow velocity and length. We choose to use mean source velocity rather than other velocities (front velocity and mass centroid velocity) because the mean source velocity only depends on the initial pressure in our experiments and does not vary with plume deformation. The front and centroid velocities are strongly influenced by water depths in addition to initial pressures, so cannot objectively reflect the source conditions. The mean source velocity represents the source kinetic energy in the eruption. With reference to Equation 3, a large Fr may signify an eruption occurring at a relatively shallow water depth (smaller denominator in Equation 3) or with a relatively strong source strength (and hence velocity, larger numerator in Equation 3). A small Fr signifies the opposite, that is a relatively deep water depth and/or a relatively weak source strength (and hence velocity). Therefore, the Froude number is a non-dimensional parameter combining the water depth

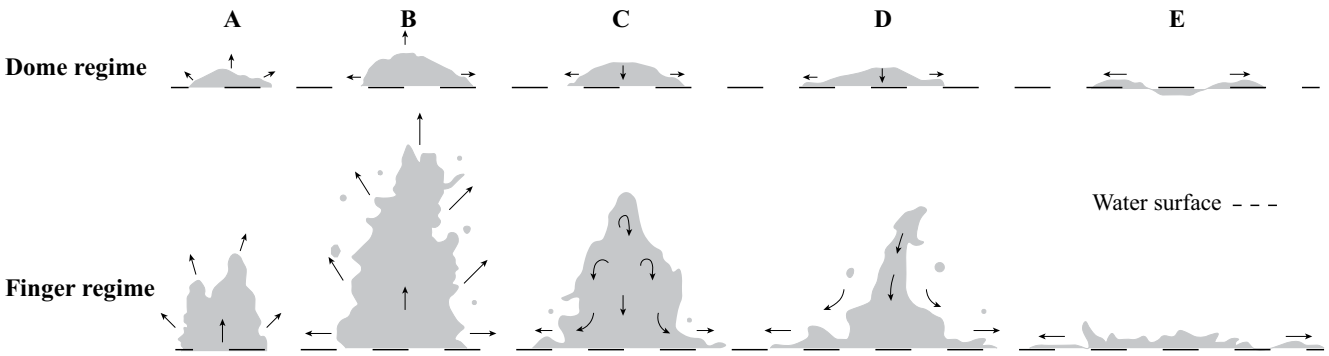

Figure 7. Cartoon schematics of the evolution of two fountain evolution regimes (dome shape and finger shape) observed in the experiments. A and B are ejecting stage; C and D are falling stage; E shows the wave propagation. The arrows indicate the direction of motion of the fountains and waves.

and source intensity. In order to quantify the fountain regimes, we use the aspect ratio of the core fountain, when it reaches the highest point (0.34–0.98 s). This characteristic aspect ratio A (Equation 4) is defined by the ratio of the maximum height of a fountain H_f to the fountain's diameter at the water surface D_f (used to differentiate this from the water depth, d).

$$A = \frac{H_f}{D_f} \tag{4}$$

H_f and D_f can be obtained by the fountain boundary-detecting algorithm in Section 3.2. We do not consider whether the fountain is axisymmetric in the calculation, although the calculation implicitly assumes that on average the shape will be symmetrical. A dome-shaped fountain is low and wide, i.e., the aspect ratio is small, while the opposite is true for a finger-shaped fountain.

Mean source velocity and water depth represent the impetus factor and resistance factor for fountain generation, respectively. A larger Fr corresponds to a higher fountain (in the finger regime), while a lower Fr corresponds to a lower fountain (in the dome regime). There is a positive linear correlation between the Fr and the aspect ratio of the fountain (Figure 8a). When the Fr is below 4.6, the aspect ratio is zero, which means there is a negligible disturbance created by the fountain at the free surface. In reality, for the hot and condensable plumes, the condensation and dissolution of plumes as it rises would further decrease the gas volume and reduce the efficiency of fountain generation. When the Fr is larger than 4.6, three main types of fountains can be approximately classified: a dome regime ($4.6 < Fr < 7.5$); a transitional regime ($7.5 < Fr < 10.5$); and a finger regime ($Fr > 10.5$). There are two limiting cases here: (a) When the Fr tends to 0 (infinite water depth), there is no fountain generated on the water surface, because the energy is lost during the plume's motion. (b) When the Fr tends to positive infinity (water depth close to 0), most energy would be dissipated into the air. This eruption would just generate some splashes and no core fountain would occur in this case. Therefore, we posit that there is an optimal Froude number between zero and infinity where efficiency of fountain generation is maximum. Based on our experimental data, we infer that the range of the optimal Fr is between 7.5 and 10.5 (i.e., within the transitional regime), as there is a large amount of energy loss in the water column and the air in dome regimes ($Fr < 7.5$) and finger regimes ($Fr > 10.5$), respectively.

In underwater explosion experiments, Stepanov and Navagin (1966) similarly found that the maximum mass of water above the explosion center could be collected when explosions took place at a critical water depth. The mass of displaced water represents the potential energy in the fountain. Although our approach is different to the approach in Stepanov and Navagin (1966)'s experiments, where the depth of the explosion was varied within the water column, both approaches lead to the conception of an optimal initiation depth for fountain generation. In on-land subsurface explosion experiments, a scaled depth $D_{sc} = dE^{-1/3}$ has been proposed to describe the regimes of explosion; where d is the physical depth and E is the mechanical energy generated by the explosion. For a given energy, there is an optimum depth (0.003–0.004 m $\cdot$J$^{-1/3}$) where an explosion will generate maximum crater size, and there is a containment depth (0.008 m $\cdot$J$^{-1/3}$) below which an explosion will be entirely contained below the surface (Valentine et al., 2014). This cratering research (Valentine et al., 2014) strongly supports our recognition of the different fountain regimes based on the Fr. The Fr cannot be directly applied to the onland cratering experiments, because the explosive energy and materials are transmitted radially in all directions from an explosive source and it is difficult to measure the source velocities in underground explosion experiments. The denominator of the Fr corresponds to the propagation velocity of a shallow-water wave in a given water depth (Holthuijsen, 2010). It is also difficult to define an equivalent velocity based on the depth of explosion in the onland context.

4.4. Application

Dimensionless parameters (the Fr and the aspect ratio of the fountain) allow testing the applicability of our experimental relationship (Figure 8a) to field events with known water depths and fountain dynamics (e.g., where a video or a series of photographs records the fountain evolution and its aspect ratio at the highest point). As there are no direct measurements of the source velocities in all historical events, we can only estimate the source velocities based on the fountain velocities (calculated from the gradient of the fountain

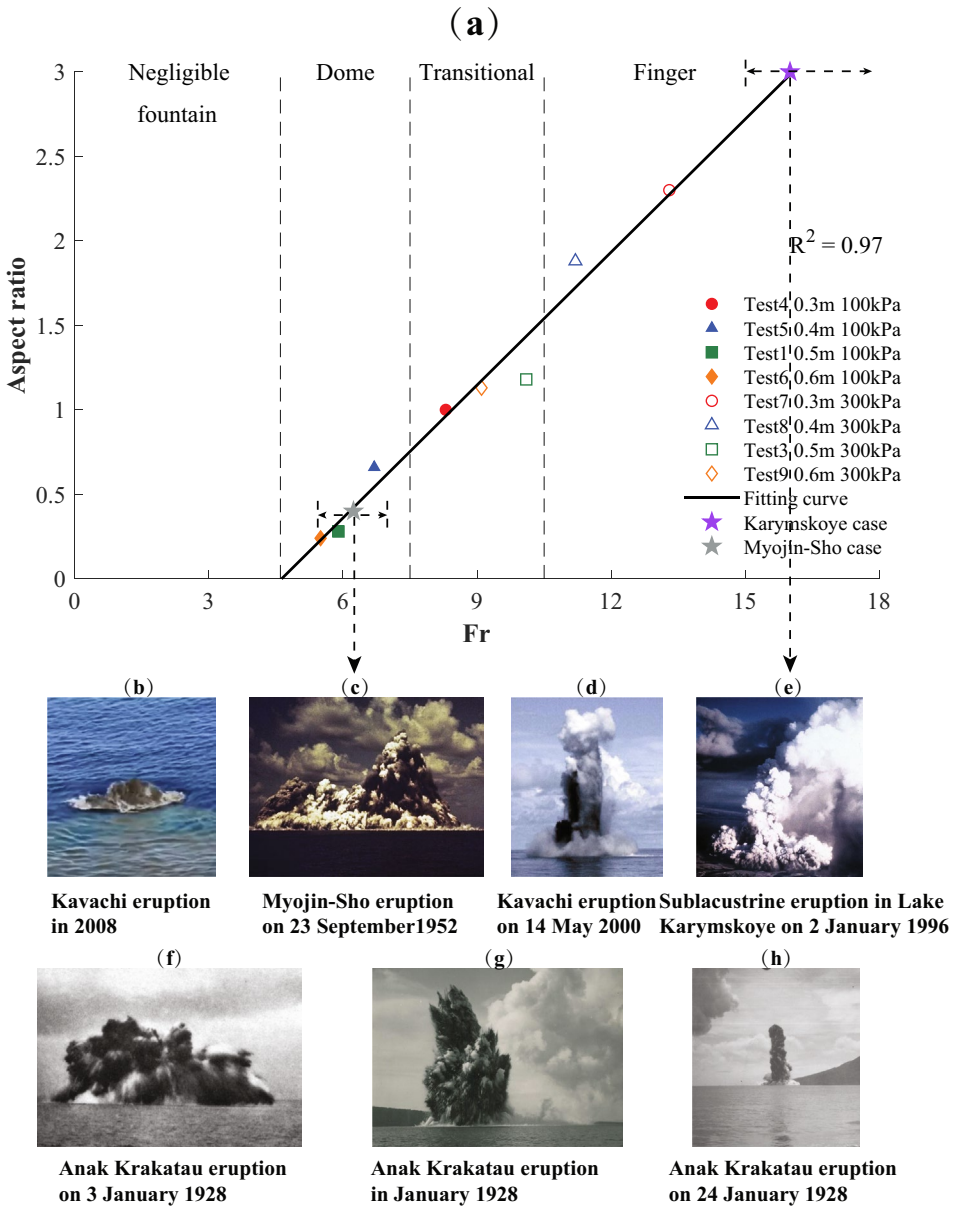

Figure 8. (a) The relationship between the Froude number and the aspect ratio of the fountain; (b) Negligible fountain: Kavachi eruption in 2008 (BBC Natural History Unit (2009)); (c) Dome regime: Myojin-Sho eruption on September 23, 1952 (Ryohei Morimoto photograph; Figure in Global Volcanism Program (2013)); (d) Finger regime: Kavachi eruption on May 14, 2000 (R. Arculus photograph; Figure 2 in Baker et al. (2002)); (e) Finger regime: Subacustrine eruption in Karymskoye lake on January 2 , 1996 (Ya. D. Muraviev photograph; Figure 3b in Belousov and Belousova (2001)); (f) Dome regime: Anak Krakatau eruption on January 24 ,1928 (Umbgrove photograph; Figure 5 in Umbgrove (1928)); (g) Transitional regime: Anak Krakatau eruption in January, 1928 (Stehn photograph; Figure 57 in Krippner and Venzke (2019)); (h) Finger regime: Anak Krakatau eruption on January 24, 1928 (Stehn photograph; Figure 16 in Stehn (1929)).

front path). In our experimental results, the source velocities (calculated in Tabel 1) are approximately three times larger than the maximum fountain velocities (calculated from the gradient on Figure 4). We assume this relationship between source velocity and maximum fountain velocity also holds in the field, and thus we can estimate the source velocities and the Fr of the field cases.

In mid-September,1952, Myojin-Sho Reef erupted several times and tsunamis generated by these submarine explosions were recorded by a wave gauge installed on Hachijio Island about 130 km north of the reef

(Miyoshi & Akiba, 1954; Nakano et al., 1954). One eruption, which occurred at 13:12 JST on September 23, was witnessed from at about 1.8 km distance from the source epicenter, and well-recorded in a series of photos that shows the whole process of water dome motion on the free surface (Morimoto, 1960). Based on the estimated height and width of the water plumes in these photos, the aspect ratio of the water plumes in this eruption was lower than 0.4, and hence belongs to a dome regime (Figure 8a). The maximum fountain velocity calculated from this series of photos is about 54 m/s. The volcano vent was at a depth of 50–100 m (Fiske et al., 1998; Morimoto, 1960). Therefore, the estimated Fr for the Myojin-Sho case is between 5.17 and 7.3 (Figure 8a), which is below the optimal range of Froude number. The eruption energy must have been weak because it only created a dome, even in this shallow water. This September 23 eruption with relatively low fountain energy did not generate large-amplitude waves, unlike eruptions that occurred on the September 16, 24, and 26 which generated tsunamis that were recorded at Hachijo Island (130 km from source). The lack of an observed tsunami on the September 23 is consistent with the conclusions of our model that the eruption was low-energy.

In 1996, a series of subaquatic phreatomagmatic eruptions occurred in Lake Karymskoye, Russia from an initial water depth about 50 m (Belousov & Belousova, 2001). The development of one of the strongest explosions above the water surface was well recorded by a video (Muraviev et al., 1997) and described by Belousov and Belousova (2001). The process of the eruption in Lake Karymskoye (Figure S1) is qualitatively consistent with our experimental results (Belousov & Belousova, 2001). Based on our classification on the fountain regimes (Figure 7), the regime of the eruption in Lake Karymskoye appears to be in the finger regime (Figure 8e), which means this eruption occurred at relatively shallow water depth and with strong source energy. This particular eruption occurred about three hours after the beginning of the eruption in Lake Karymskoye, and the vent depth was shallower than 50 m, because a large amount of pyroclastic material consisting mainly of juvenile basalts was deposited near the vent (Belousov & Belousova, 2001; Muraviev et al., 1997;). The maximum velocity of the fountain was about 110 m/s (Belousov & Belousova, 2001). Therefore, the estimated Fr of the eruption in the Lake Karymskoye will be greater than or equal to 15, which places it in the finger regime in our analysis. As the upper boundary of the estimated Fr can be positive infinity (water depth tends to zero), it is difficult to constrain the upper limit of the error bar and therefore we have not included an upper boundary of the Fr in Figure 8a. The aspect ratio of the fountain in this case is about 3 (maximum height 1 km with a width of about 330 m). In reality, the water depth at this time during the eruption would have been shallower than 50 m. Nevertheless, this field case also fits reasonably well with our experimental data (Figure 8a).

There are some limitations in our calculations. When we estimate the Fr of the real cases, we assume that the relationship between the source velocities and the fountain velocities is the same as in our physical experiments, which may not be the case. When we estimate the fountain velocity, height and width in the field cases based on photos or videos, two main factors would contribute to the errors in the calculated Fr and the aspect ratios of the fountains. Firstly, the eruptive ash and steam would mask the actual water dome and artificially increase the observed heights and widths. Secondly, the recording angle and relatively low resolution of pictures would also increase the error in the final results.

We have qualitatively analyzed images and videos from a further two eruptions. However, image quality and a lack of information about important parameters, such as water depths and velocities limit the analysis that can be done using our model. Anak Krakatau volcano had several submarine eruptions in January 1928 and some fountains produced by these eruptions were recorded by Umbgrove (1928) and Stehn (1929). These eruptions all occurred at approximately the same vent depth (about 25 m). Stehn (1929) observed that three shapes of water domes or fountains appeared on the surface: “upwelling of water” (Figure 8f), “water-cones” (Figure 8g), and “columns” (Figure 8h), as the explosive intensities changed from weak explosions to violent explosions (depth relative to the energy changed from high to low). These field observations are consistent with our experimental fountain regimes that dome regimes, transitional regimes, and finger regimes are observed successively when the Fr number increases from low to high (depth relative to the energy changes from high to low). The fountain generated by Kavachi eruption, Solomon Island in 2008 produced negligible surface deformation suggesting a Froude number below 4.6 (Figure 8b) (BBC Natural History Unit, 2009). The fountains generated in Kavachi eruption on May 14, 2000 belong to the finger regime (Figure 8d).

5. Conclusions

We developed physical experiments to simulate fountains generated by underwater discrete eruptions, and quantitatively recorded and analyzed the motion of gas injected into water as a momentum jet that evolves into a buoyant plume and fountains at the water surface. Three fountain regimes (a dome regime, a finger regime and a transitional regime) are observed and classified by the Froude number in the experiments. These regimes are consistent with the fountains observed in the field during submarine volcanic eruptions. The fountain generated by the Myojin-Sho submarine volcanic eruption on September 23, 1952 belonged to a dome regime, which means it was a weak-source eruption. The 1996 underwater volcanic eruption in Lake Karymskoye was categorized as the finger regime, which means it was a shallow and strong-source eruption.

This research is a valuable initial step in gaining a better understanding of how underwater volcanic eruptions may produce tsunamis. Future research could account for the thermal contraction of the erupted gas, for example by using water vapor instead of compressed air in physical experiments. This would allow an assessment of the role of condensation in jet-plume motion and associated fountain generation. Some constant parameters in the present study could also be modified in future studies, such as the diameter of the vent and the eruption duration. Further investigation of the characteristics of waves generated by the collapse of the fountain is also required to complete our knowledge of the initiation process of a submarine volcanic tsunami.

Data Availability Statement

The initial conditions and source data presented in this research are provided in Table 1. The mean plume-jet boundary data, water surface profile data and two MATLAB scripts to visualize them are available at https://doi.org/10.5281/zenodo.4615689.

Acknowledgments
The funding for this research was supported by the Marsden grants NIW1703. Yaxiong Shen acknowledges funding from the University of Auckland Doctoral Scholarship. We are very grateful for the careful and thoughtful reviews of Rebecca Williams and two anonymous reviewers, as well as the very helpful suggestions of the editor, Ryan P. Mulligan. The authors wish to express their gratitude to Natalia Lipiejko, Bruce William Melville, Stephane Popinet, Asaad Yahia Shamseldin, Liam Wotherspoon, N.A.K. Nandasena, and Graham Macky for their helpful comments. We also thank Ninger Kong, Geoffrey Kirby, Dan William Fray, Oane Galama, Jos Geurts, Trevor Patrick, and Lee Walker-Holt for help while preparing the experiments.

References

Alatorre-Ibargüengoitia, M. A., Scheu, B., & Dingwell, D. B. (2011). Influence of the fragmentation process on the dynamics of vulcanian eruptions: An experimental approach. *Earth and Planetary Science Letters*, *302*(1–2), 51–59. https://doi.org/10.1016/j.epsl.2010.11.045

Baker, E. T., Massoth, G. J., de Ronde, C. E. J., Lupton, J. E., & McInnes, B. I. A. (2002). Observations and sampling of an ongoing subsurface eruption of Kavachi volcano, Solomon Islands, May 2000. *Geology*, *30*(11), 975–978. https://doi.org/10.1130/0091-7613(2002)030<0975:oasoao>2.0.co;2

BBC Natural History Unit, S. (2009). *Ocean of volcanoes (bbc south pacific/discovery wild pacific series)*. Retrieved from https://vimeo.com/groups/techteachers/videos/27407450

Belousov, A., & Belousova, M. (2001). Eruptive process, effects and deposits of the 1996 and ancient basaltic phreatomagmatic eruptions in Karymskoye lake, Kamchatka, Russia. *Special Publications of the International Association of Sedimentologists*, *30*, 35–60.

Bernard, L. M., & Shen, W. (1996). Water Waves Generated by Underwater Explosion. Vol. 10. World Scientific.

Bie, H.-Y., Ye, J.-J., & Hao, Z.-R. (2016). Effect of nozzle geometry on characteristics of submerged gas jet and bubble noise. *Journal of Laboratory Automation*, *21*(5), 652–659. https://doi.org/10.1177/2211068215584902

Bombrun, M., Jessop, D., Harris, A., & Barra, V. (2018). An algorithm for the detection and characterization of volcanic plumes using thermal camera imagery. *Journal of Volcanology and Geothermal Research*, *352*, 26–37. https://doi.org/10.1016/j.jvolgeores.2018.01.006

Cashman, K. V., & Fiske, R. S. (1991). Fallout of pyroclastic debris from submarine volcanic eruptions. *Science*, *253*(5017), 275–280. https://doi.org/10.1126/science.253.5017.275

Chadwick, W., Jr, Cashman, K., Embley, R., Matsumoto, H., Dziak, R., De Ronde, C., & Merle, S. (2008). Direct video and hydrophone observations of submarine explosive eruptions at NW Rota-1 volcano, Mariana arc. *Journal of Geophysical Research*, *113*(B8). B08S10. https://doi.org/10.1029/2007jb005215

Chojnicki, K. N., Clarke, A. B., Phillips, J. C., & Adrian, R. J. (2015). Rise dynamics of unsteady laboratory jets with implications for volcanic plumes. *Earth and Planetary Science Letters*, *412*, 186–196. https://doi.org/10.1016/j.epsl.2014.11.046

Clarke, A.B., Phillips, J.C., & Chojnicki, K.N. (2009). An investigation of vulcanian eruption dynamics using laboratory analogue experiments and scaling analysis. In T. Thordarson, S. Self, G. Larsen, S. K. Rowland, & A. Hoskuldsson (Eds.), *Studies in Volcanology* (Vol. 2, 155–166). London, UK: Geological Society of London.

Day, S. J. (2015). Volcanic tsunamis. In *The encyclopedia of volcanoes*. 993–1009. Elsevier. https://doi.org/10.1016/b978-0-12-385938-9.00058-4

Deardorff, N. D., Cashman, K. V., & Chadwick, W. W., Jr (2011). Observations of eruptive plume dynamics and pyroclastic deposits from submarine explosive eruptions at NW Rota-1, Mariana arc. *Journal of Volcanology and Geothermal Research*, *202*(1–2), 47–59. https://doi.org/10.1016/j.jvolgeores.2011.01.003

Dietz, R. S., & Sheehy, M. J. (1954). Transpacific detection of Myojin volcanic explosions by underwater sound. *The Geological Society of America Bulletin*, *65*(10), 941–956. https://doi.org/10.1130/0016-7606(1954)65[941:tdomve]2.0.co;2

Fiske, R. S., Cashman, K. V., Shibata, A., & Watanabe, K. (1998). Tephra dispersal from Myojinsho, Japan, during its shallow submarine eruption of 1952-1953. *Bulletin of Volcanology*, *59*(4), 262–275. https://doi.org/10.1007/s004450050190

Fouqué, F. (1879). *Santorin et ses éruptions*. Paris: Masson et Compagnie.

Global Volcanism Program, S. (2013). Global volcanism [program, 2013. Report on Myojinsho *Bulletin of the Global Volcanism Network*. Retrieved from https://volcano.si.edu/volcano.cfm?vn=284070&vtab=Bulletin#bgvn_197004

Global Volcanism Program, S. (2014). Global volcanism program, 2014. Report on Kavachi (Solomon Islands). *Bulletin of the Global Volcanism Network*, 39(7).
Holthuijsen, L. H. (2010). *Waves in oceanic and coastal waters*. Cambridge university press.
Kedrinskiy, V. K. (2006). *Hydrodynamics of explosion: Experiments and models*. Springer Science & Business Media.
Krippner, J., & Venzke, E. e. (2019). Global volcanism program, 2019. Report on Krakatau (Indonesia). *Bulletin of the Global Volcanism Network*, 44(3).
Latter, J. H. (1981). Tsunamis of volcanic origin: Summary of causes, with particular reference to Krakatoa, 1883. *Bulletin Volcanologique*, *44*(3), 467–490. https://doi.org/10.1007/bf02600578
Mader, H. M., Zhang, Y., Phillips, J. C., Sparks, R. S. J., Sturtevant, B., & Stolper, E. (1994). Experimental simulations of explosive degassing of magma. *Nature*, *372*(6501), 85–88. https://doi.org/10.1038/372085a0
Mastin, L., & Witter, J. (2000). The hazards of eruptions through lakes and seawater. *Journal of Volcanology and Geothermal Research*, *97*(1–4), 195–214. https://doi.org/10.1016/s0377-0273(99)00174-2
Maurel, A., Cremer, S., & Jenffer, P. (1997). Experimental study of a submerged fountain. *Europhysics Letters*, *39*(5), 503–508. https://doi.org/10.1209/epl/i1997-00384-1
Miyoshi, H. (1955). Explosion waves accompanying the eruptions of Myojin Reef. *Journal of the Oceanographical Society of Japan*, *11*(4), 157–163. https://doi.org/10.5928/kaiyou1942.11.157
Miyoshi, H., & Akiba, Y. (1954). The tsunamis caused by the Myojin explosions. *Journal of the Oceanographical Society of Japan*, *10*(2), 49–59. https://doi.org/10.5928/kaiyou1942.10.49
Morimoto, R. (1960). Submarine eruption of the Myôjin reef. *Bulletin Volcanologique*, *23*(1), 151–160. https://doi.org/10.1007/bf02596641
Munson, B. R., Okiishi, T. H., Huebsch, W. W., & Rothmayer, A. P. (2013). *Fluid mechanics*. Wiley Singapore. https://doi.org/10.4324/9781315821368
Muraviev, Y. D., Fedotov, S. A., Budnikov, V. A., Ozerov, A. Y., Maguskin, M. A., Dvigalo, V. N., et al. (1997). The 1996 volcanic activity in the Karymskii center: The summit eruption of Karymskii volcano and the phreatomagmatic eruption in the Akademii Nauk Caldera. *Volcanology and Seismology*, (5), 38–70.
Nakano, M., Unoki, S., Hanzawa, M., Marumo, R., & Fukuoka, J. (1954). Oceanographic features of a submarine eruption that destroyed the Kaiyo-Maru No. 5. *Journal of Marine Research*, *13*, 48–66.
Ozawa, Y., & Mori, K. (1986). Effect of physical properties of gas and liquid on bubbling-jetting phenomena in gas injection into liquid. *ISIJ International*, *26*(4), 291–297. https://doi.org/10.2355/isijinternational1966.26.291
Resing, J. A., Rubin, K. H., Embley, R. W., Lupton, J. E., Baker, E. T., Dziak, R. P., et al. (2011). Active submarine eruption of boninite in the northeastern Lau Basin. *Nature Geoscience*, *4*(11), 799–806. https://doi.org/10.1038/ngeo1275
Sangras, R., Kwon, O. C., & Faeth, G. M. (2002). Self-preserving properties of unsteady round nonbuoyant turbulent starting jets and puffs in still fluids. *Journal of Heat Transfer*, *124*(3), 460–469. https://doi.org/10.1115/1.1421047
Shen, Y., Whittaker, C. N., Lane, E. M., White, J. D. L., Power, W., & Nomikou, P. (2021). Laboratory experiments on tsunamigenic discrete subaqueous volcanic eruptions. Part 2: Properties of generated waves. *Journal of Geophysical Research: Oceans*, *126*, e2020JC016587. https://doi.org/10.1029/2020JC016587
Stehn, C. E. (1929). *The geology and volcanism of the Krakatau group*. In Proceedings of the Fourth Pacific science congress,pp. 1–55.
Stepanov, V., & Navagin, Y. (1966). Hydroexplosive pressing of ship units. Sudostroenie, Leningrad.
Umbgrove, J. H. F. (1928). The first days of the new submarine volcano near Krakatoa. *Leidse Geologische Mededelingen*, *2*(1), 325–328.
Valentine, G. A., Graettinger, A. H., & Sonder, I. (2014). Explosion depths for phreatomagmatic eruptions. *Geophysical Research Letters*, *41*(9), 3045–3051. https://doi.org/10.1002/2014gl060096
Verolino, A., White, J. D. L., & Zimanowski, B. (2018). Particle transport in subaqueous eruptions: An experimental investigation. *Journal of Volcanology and Geothermal Research*, *349*, 298–310. https://doi.org/10.1016/j.jvolgeores.2017.11.013
Walker, S. L., Baker, E. T., Resing, J. A., Chadwick, W. W., Lebon, G. T., Lupton, J. E., & Merle, S. G. (2008). Eruption-fed particle plumes and volcaniclastic deposits at a submarine volcano: NW Rota-1, Mariana Arc. *Journal of Geophysical Research*, *113*(B8). https://doi.org/10.1029/2007jb005441
Witze, P. O. (1983). Hot-film anemometer measurements in a starting turbulent jet. *AIAA Journal*, *21*(2), 308–309. https://doi.org/10.2514/3.8071
Wohletz, K. H. (1986). Explosive magma-water interactions: Thermodynamics, explosion mechanisms, and field studies. *Bulletin of Volcanology*, *48*(5), 245–264. https://doi.org/10.1007/bf01081754
Wohletz, K. H., & McQueen, R. G. (1984). Experimental studies of hydromagmatic volcanism. *Explosive volcanism: Inception, evolution, and azards*, 158–169.
Wraith, A., & Chalkley, M. (1977). Advances in extractive metallurgy, ed. by M.J. jones. *IMM, London*, 27.